

Reaction Chemistry & Engineering

Linking fundamental chemistry and engineering to create scalable, efficient processes

Accepted Manuscript

This article can be cited before page numbers have been issued, to do this please use: Y. Qiu, I. Conti, E. Berretti and A. Beretta, *React. Chem. Eng.*, 2026, DOI: 10.1039/D6RE00086J.



This is an Accepted Manuscript, which has been through the Royal Society of Chemistry peer review process and has been accepted for publication.

Accepted Manuscripts are published online shortly after acceptance, before technical editing, formatting and proof reading. Using this free service, authors can make their results available to the community, in citable form, before we publish the edited article. We will replace this Accepted Manuscript with the edited and formatted Advance Article as soon as it is available.

You can find more information about Accepted Manuscripts in the [Information for Authors](#).

Please note that technical editing may introduce minor changes to the text and/or graphics, which may alter content. The journal's standard [Terms & Conditions](#) and the [Ethical guidelines](#) still apply. In no event shall the Royal Society of Chemistry be held responsible for any errors or omissions in this Accepted Manuscript or any consequences arising from the use of any information it contains.

ARTICLE

Unprecedented promotion of NH₃ decomposition over Ru via H₂-scavenging: a chemical reaction engineering analysis

Yi Qiu,^a Ivan Conti,^a Enrico Berretti^b and Alessandra Beretta^{*a}Received 00th January 20xx,
Accepted 00th January 20xx

DOI: 10.1039/x0xx00000x

Ammonia offers great potential as hydrogen carrier, facilitating the storage, transport, and distribution of renewable energy. Nevertheless, the decomposition of ammonia, a key process for releasing hydrogen to distributed end users, represents a critical gap in the developing NH₃-based energy value chain. Two scientific issues are fully open and slow-down the process development: the catalyst formulation and the reactor design. Ruthenium is recognized as the most active metal for ammonia decomposition; however, its reactivity is strongly limited by kinetic constraints. Although the mechanistic understanding remains under debate, substantial evidence from the literature and further analysed herein through kinetic modeling demonstrates that ammonia decomposition on Ru-based catalysts is severely hindered by hydrogen inhibition. Building on this evidence, novel diagnostic tests (where the “restoring” of Ru sites was obtained by O₂ cofeeding and H₂ oxidation) and modelling (simulating the ideal condition of zero H* coverage) reveal that a huge potential is disclosed if the reactor is designed to obtain full H₂-scavenging, thus solving both the issues above mentioned. The turnover rate is shown herein to increase by a factor of 14 at 250 °C under diluted feed conditions and is projected to rise by several orders of magnitude under pure ammonia feeds at atmospheric pressure. Even greater enhancements are expected under pressurized conditions of industrial relevance.

1. Introduction

The transition toward a zero-carbon energy system requires efficient energy storage solutions capable of compensating for the intermittency of renewable power generation. While batteries are suitable for short-term storage, chemical energy storage offers a scalable option for long-term and high-capacity applications. In this framework, carbon-neutral synthetic molecules produced from renewable electricity are expected to replace fossil-derived fuels and fulfil their functional role within future energy systems.¹ In a fully decarbonized scenario, surplus renewable electricity will be employed to produce green hydrogen (H₂) via water electrolysis. Although hydrogen is an ideal carbon-free fuel, its low volumetric energy density and the technical challenges associated with its storage and transport hinder its direct large-scale use as an energy vector. To overcome these limitations, established chemical routes can convert H₂ into hydrogen-rich liquid compounds with higher energy densities.

Ammonia (NH₃) has emerged as a particularly attractive hydrogen carrier: it is carbon-free, and its production, storage, and distribution rely on a well-established global infrastructure originally developed

for fertilizer manufacturing via the Haber–Bosch process.² The development of an NH₃-based renewable energy value chain would facilitate hydrogen supply to residential, industrial, and heavy-duty transportation sectors.³ However, NH₃ decomposition has been recognized as the most technically challenging step of the entire value chain of renewable energy distribution.^{4,5} NH₃ decomposition is an endothermic reaction involving an increase in the total number of gas-phase moles; accordingly, equilibrium conversion is favoured at elevated temperatures and reduced pressures. Therefore, the attainment of appreciable conversion under practical conditions requires catalysts with high intrinsic activity. A few large-scale demonstrations of ammonia decomposition have been reported, including the industrial plant (Topsoe’s H₂RETAKE⁶) and large test facility (KIER⁷), both operating at temperatures exceeding 600°C. However, milder temperatures would be desirable to improve the overall thermal efficiency of the process, which calls for major improvements in the catalyst formulation and in the reactor design.

Ruthenium is widely recognized as the most active metal for ammonia decomposition, yet the intrinsic activity of Ru-based catalysts remains limited by both kinetic and thermodynamic constraints.^{8–11} Although the rate-determining step (RDS) has been variously attributed either to N* recombinative desorption or NH₃* activation, depending on Ru loading, support composition and operation conditions, hydrogen poisoning has been consistently identified as the main kinetic constraint.^{12–14} Ru strongly binds hydrogen, and the resulting Ru-H interactions block active sites, thereby representing a major bottleneck in NH₃ decomposition.^{15–16} Previous investigations of Ru catalysts supported on Al₂O₃, MgO, and MgAl₂O₄ under isothermal conditions revealed a pronounced inhibitory effect of H₂ partial pressure on NH₃ decomposition.¹⁷

^a Department of Energy, Politecnico di Milano, via La Masa 34, 20156 Milano.
alessandra.beretta@polimi.it

^b CNR Italian National Research Council (CNR) – Institute of Chemistry of OrganoMetallic Compounds (ICCOM), Via Madonna Del Piano 10, 50019, Sesto Fiorentino, Florence, Italy

† Footnotes relating to the title and/or authors should appear here.

Supplementary Information available: [details of any supplementary information available should be included here]. See DOI: 10.1039/x0xx00000x



Temperature-programmed desorption (H_2 -, NH_3 -, and CO_2 -TPD) analysis showed that H_2 adsorption capacity increased with support acidity ($\text{MgO} < \text{MgAl}_2\text{O}_4 < \text{Al}_2\text{O}_3$), whereas H^* associative desorption correlated with support basicity in the opposite order. The combination of moderate basicity and high Ru dispersion resulted in $\text{Ru}/\text{MgAl}_2\text{O}_4$ exhibiting the highest activity. For all catalysts, kinetics followed a simple rate law $r \propto P_{\text{NH}_3} \cdot P_{\text{H}_2}^{-1.5}$, consistent with the second N–H bond cleavage as the rate determining step and H^* as the most abundant surface intermediate. Gascon et al. similarly proposed a power-law model with reaction orders of 0.5 on NH_3 and -1.2 on H_2 for a $\text{Ru}/\text{K}-\text{CaO}$ catalyst up to 40 bar, confirming the inhibitory role of hydrogen under industrially relevant conditions.¹⁸

Building on this background, the aim of this work is to investigate and demonstrate the potential benefits of removing H^* species from the catalyst surface and H_2 from the gas phase on enhancing the rate of NH_3 decomposition over Ru catalysts. The underlying hypothesis is that selective removal of H_2 (in the following referred to as H_2 -scavenging) can mitigate surface H-poisoning effects, thereby improving overall kinetics; besides, it is expected to shift the reaction equilibrium. This concept was first assessed through detailed kinetic modelling, taking $\text{Ru}/\text{MgAl}_2\text{O}_4$ as a representative system, given its superior activity and balanced acid–base properties identified in previous studies. The model was used to quantify the influence of H_2 partial pressure and to predict the extent of rate enhancement achievable through in situ H_2 removal. Finally, these theoretical predictions were experimentally validated under controlled reaction conditions to confirm the practical impact of H_2 -scavenging on Ru-catalysed NH_3 decomposition.

2. Experimental and modelling methods

2.1 Catalyst preparation

A 1 wt.% $\text{Ru}/\text{MgAl}_2\text{O}_4$ catalyst was prepared using the incipient wetness impregnation method, employing a ruthenium nitrosyl nitrate solution from Sigma-Aldrich as precursor. The MgAl_2O_4 support was supplied by Sasol Germany GmbH. A two-step impregnation procedure was adopted, with overnight drying in air at 120 °C between the two impregnation steps. After the final impregnation, the material was dried overnight at 120 °C and subsequently calcined up to 500 °C by heating from room temperature to 500 °C at a rate of 1 °C min⁻¹, followed by a dwell time of 5 h at the final temperature. The resulting material was then sieved, and the 140–200 mesh fraction, corresponding to particle sizes between 75 and 106 μm, was selected for catalytic testing.

2.2 Catalyst characterization

The effective Ru loading of the catalyst was verified by ICP–OES after acid digestion using a PerkinElmer Optima 8300 instrument. Measurements were performed on both fresh and spent samples after catalytic tests under NH_3 and $\text{NH}_3 + \text{O}_2$ atmospheres. Prior to the characterization of spent catalysts, the samples were passivated under a 1% O_2 flow at 30 °C for 1 h to prevent uncontrolled oxidation upon exposure to air.

X-ray diffraction (XRD) patterns of both fresh and spent catalysts were recorded using a PANalytical Empyrean diffractometer

operating in Bragg–Brentano geometry and equipped with a copper X-ray source (Cu K α radiation). Data were collected in continuous scanning mode over a 2 θ range of 20°–80°.

Morphological and structural characterization of fresh and spent catalysts was performed using a Thermo Fisher Scientific Talos F200X G2 transmission electron microscope operating at an accelerating voltage of 200 kV. Scanning Transmission Electron Microscopy (STEM), Scanning Transmission Electron Microscopy - Energy Dispersive X-ray Spectroscopy (STEM-EDX), and High-Resolution Transmission Electron Microscopy (HRTEM) modes were employed to characterize the samples. Sample preparation followed a conventional three-step procedure: (i) dispersion of a small amount of sample powder in isopropanol, (ii) sonication, and (iii) drop-casting of the suspension onto Cu holey TEM grids.

2.3 Catalytic tests in microreactor

300 mg catalyst diluted with 300 mg quartz powder of the same particle size was loaded into a micro fixed-bed quartz reactor (i.d. 8mm). Prior to catalytic testing, the catalyst was pre-reduced under a 1% H_2/Ar flow by heating from room temperature to 450 °C at a rate of 5 °C/min, followed by a 1 h hold. During catalytic experiments, a thermocouple independent of the over controller was positioned at the centre of the catalyst bed to directly measure the actual bed temperature. The gas mixture at reactor outlet was analysed by a ThermoStar quadrupole mass spectrometer (Pfeiffer Vacuum).

The entire kinetic investigation was performed at a gas hourly space velocity (GHSV) of 20,000 $\text{NI}/\text{kg}_{\text{cat}}/\text{h}$, which allowed to explore a wide range of conversions at varying feed composition in the temperature range 250–450 °C.

As described in our previous work, experiments were performed at varying temperature and feed composition¹⁷. In particular, NH_3 decomposition experiments were performed at varying NH_3 concentration in the range 0.3–2.5% (in He); the effect of H_2 co-feed was tested in the range 1–25%.

In this work, H_2 oxidation experiments were also performed by feeding 0.5% H_2 with 0.5% O_2 in He flow. Temperature was varied from 110 °C to 235 °C.

O_2 cofeeding tests were then conducted at a fixed NH_3 concentration of 1%, while the O_2 concentration was varied between 0.05% and 0.25%. Helium was adopted for dilution. The O_2 level was intentionally kept low to minimize any potential influence from the heat release associated with the exothermic H_2 oxidation.

2.4 Temperature-programmed desorptions

Temperature-programmed experiments under He (TPD), H_2/He (TPR) and O_2/He (TPO) flows were performed to identify and quantify the adsorbed species after representative pre-treatments of the catalyst.

2.4.1 TPD

The pre-reduced catalyst was first treated at 250 °C for 1 h with 100 Nml/min flow of either 1% NH_3 or 1% $\text{NH}_3 + 0.25\% \text{O}_2$ in He. The samples were then purged with pure He at 250 °C for 1 h and cooled to 50 °C under the same flow. Subsequently, the temperature-programmed desorption was initiated at 50 °C and up to 450 °C with



a heating rate of 5 °C/min and a 1 h hold at the maximum temperature.

2.4.2 TPO

The TPO experiments were carried out by feeding 0.1% O₂/He to the pre-reduced catalyst at room temperature, and heating from room temperature to 450°C with heating rate 5°C/min, holding for 1h.

2.4.3 TPR

The pre-reduced catalyst was first treated at 250 °C for 1 h under a 100 Nml/min flow of either 1% NH₃, 1% NH₃ + 0.25% O₂ or 0.25% O₂ in He. The samples were subsequently purged with He at 250 °C for 1 h and cooled to 50 °C under the same flow. The feed was then switched to 0.5 % H₂/He, and the temperature-programmed reduction was carried out from 50 °C to 450 °C at a heating rate of 5 °C/min, and the reactor was held at 450 °C for 1 h.

2.5 Reactor modelling

The reactor behaviour was simulated using the one-dimensional pseudo-homogeneous plug flow reactor model reported in Eq. 1. The model consists of a system of differential atomic balance equations for each reacting species *i*, expressed as a function of the reaction rates *j*. Coherently with the experimental conditions, isothermal and isobaric operation was assumed.

$$\frac{dF_i}{dW_{cat}} = \sum_{j=1}^n \nu_{i,j} \cdot r_j \quad (\text{Eq. 1})$$

Where:

- F_i [mol/s] is the molar flow rate of species *i*
- W_{cat} [g_{cat}] is the catalyst weight, used as the axial coordinate
- $\nu_{i,j}$ is the stoichiometric coefficient of species *i* in reaction *j*
- r_j [mol/s/g_{cat}] is the rate of the reaction *j*
- *n* is the number of reactions that occur inside the reactor

The mass balances reported in Eq. 1 were coupled with the boundary conditions in Eq. 2:

$$F_i(W_{cat} = 0) = X_i \cdot 10^{-6} \cdot F_{tot}(W_{cat} = 0) \quad (\text{Eq. 2})$$

$$F_{tot}(W_{cat} = 0) = \frac{GHSV \cdot W_{cat}}{22.414 [Nl/mol] \cdot 1000 [Nml/Nl] \cdot 3600 [s/h]} \quad (\text{Eq. 3})$$

Where:

- $F_i(W_{cat} = 0)$ [mol/s] is the inlet molar flow rate of species *i*
- X_i [ppm] is the inlet concentration of species *i*
- $F_{tot}(W_{cat} = 0)$ [mol/s] is the total inlet molar flow rate (Eq.3)
- GHSV [Nml/g/h] is the gas hourly space velocity
- W_{cat} [g] is the total catalyst load

The system of equations was solved numerically by means of two tools: the command ode45 available in MATLAB and the Fortran subroutine LSODI. The adapted parameters for the expressions of the rates of reaction were estimated through a non-linear regression performed by the Fortran subroutine BURENL based on the least-squares method, which provided also useful statistical indexes such as the correlation matrix of the parameters and their intervals of confidence.

3. Results and Discussion

View Article Online

DOI: 10.1039/D6RE00086J

3.1 Partially adjusted reaction rate equation

The rate equation originally obtained by Qiu et al.¹⁷ was re-written in the form:

$$r = k(T) \cdot P_{NH_3} \cdot (1 + k_{H_2} P_{H_2})^{-1.5} \cdot (1 - \eta) \quad (\text{Eq. 4})$$

$$\eta = K_p \cdot K_{eq}^{-1}(T) = \frac{P_{N_2}^{0.5} \cdot P_{H_2}^{1.5}}{P_{NH_3}} \cdot K_{eq}^{-1}(T)$$

where the term $(1 - \eta)$ accounts for thermodynamic consistency and consists in the ratio between reaction quotient and equilibrium constant, calculated with the correlations by Gillespie and Beattie.¹⁹

The modified Eq. 4 has no direct mechanistic derivation but reflects the correct kinetic dependences and is numerically more robust than the original power-law model. Eq. 4 was incorporated in the isothermal pseudo-homogeneous reactor model of the lab-scale micro fixed bed reactor and adapted to the Ru/MgAl₂O₄ data (sets of experiments at varying NH₃ concentration, at varying H₂ and N₂ co-feed with constant NH₃ concentration, and at varying NH₃ concentration at fixed H₂ co-feed). Fig. 1 and 2 present the model fit to experimental data illustrating the effects of NH₃ feed concentration and H₂ cofeeding. The results reveal an apparent self-inhibiting behaviour of ammonia, with conversion shifting to progressively higher temperatures as the NH₃ concentration increases. This trend can be attributed to H₂ poisoning, as clearly evidenced by the H₂ cofeed experiments. The observed compositional dependencies are well reproduced by the modified power-law kinetic model. Fig. 1 also reports the extrapolated simulation of conversion versus temperature up to the condition of a pure NH₃ feed. The inhibitory effect of hydrogen is substantial, with the conversion curve shifting markedly toward higher temperatures when moving from diluted to concentrated NH₃ feeds. In the latter case, given the large extrapolation from the experimental campaign on the Ru/MgAl₂O₄ catalyst, for qualitative comparison, the performance of a commercial Heraeus Ru catalyst tested in an independent study was included.²⁰



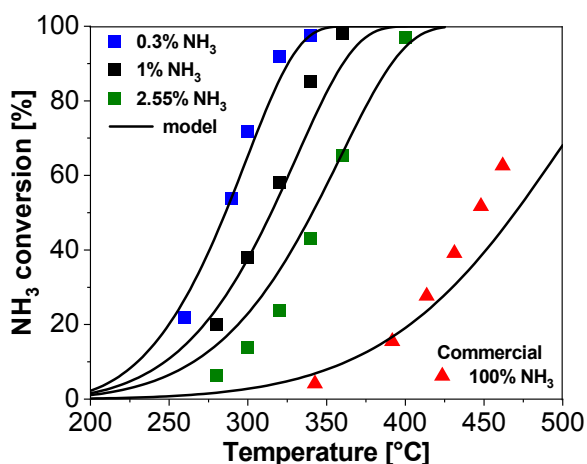


Fig. 1 Effect of NH_3 concentration, experimental data (symbols) and modelling results (solid lines) with parameters in Eq. 4: $k(600\text{K}) = 3.64\text{e-}2 \text{ mol/s/g}_{\text{cat/atm}}$; $E_{\text{act}} = 37.5 \text{ kcal/mol}$; $K_{\text{H}_2} = 5\text{e}3 / \text{atm}$.

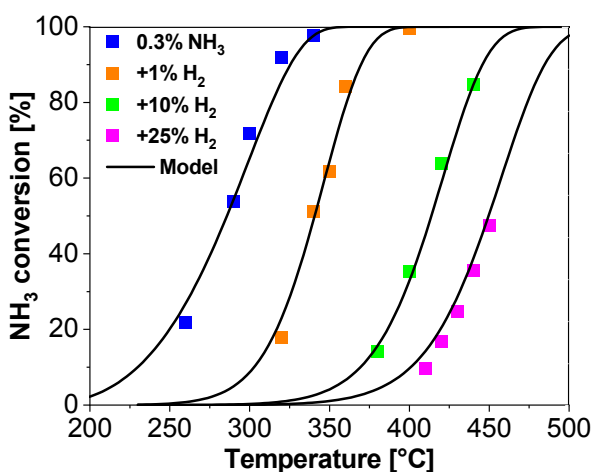


Fig. 2 Effect of H_2 cofeeding, experimental data (symbols) and modelling results (solid lines) with the same parameters in Eq. 4 as in Fig. 1.

3.2 Prediction of ideal H-scavenging

To predict the ideal performance with full H_2 removal from the surface and the reactor (i.e. the virtual condition of zero H^* coverage and no thermodynamic limitation), the assumptions $K_{\text{H}_2} = 0$ and $\eta = 0$ were applied in Eq. 4. The model prediction for a 1% NH_3 feed is shown in Fig. 3 as the blue line, which reveals a dramatic improvement of the reactor performance compared to the modelled and experimentally measured H_2 -inhibited response of the catalyst (black line). The modelling results indicate that, under complete H_2 scavenging, full NH_3 conversion can be attained at 250 °C even at a GHSV of 20,000 $\text{NI/kg}_{\text{cat/h}}$ corresponding to a 14-fold increase in the catalyst's intrinsic activity at this temperature (as quantified in Table S1). This level of enhancement surpasses the improvements reported in the extensive literature on advanced Ru-based formulations.¹⁵ Furthermore, simulations of the clean catalyst surface reveal that, in the absence of H_2 inhibition, the reaction rate depends solely on NH_3 activation. Consequently, the calculated ammonia conversion

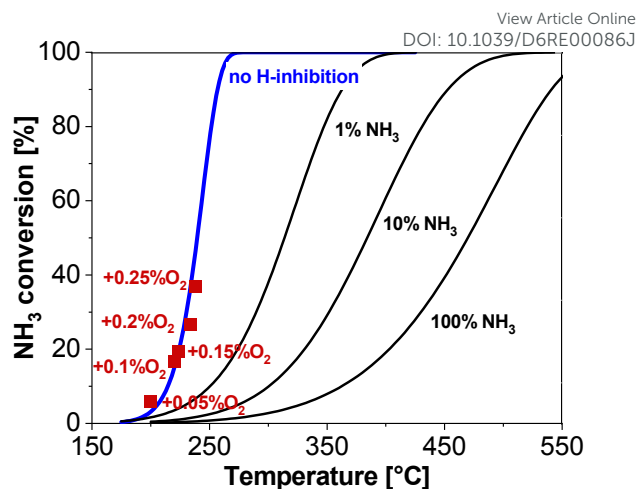


Fig. 3 Predicted NH_3 conversion in the absence of H-inhibition (blue curve) and under H-inhibited conditions (black curves), together with experimental data for 1% NH_3 with 0.05–0.25% O_2 cofeed (red squares), $\text{GHSV} = 20000 \text{ NI/h/kg}_{\text{cat}}$.

becomes independent of NH_3 concentration. In other words, the predicted blue line applies not only to the highly diluted 1% NH_3 feed but also to concentrated NH_3 . Under these conditions, the enhancement factor of the catalyst activity at 250 °C increases enormously: it exceeds 50 at 10% NH_3 feed and surpasses 600 for pure NH_3 feed, corresponding to a reduction of over 300 °C in the temperature required for complete NH_3 conversion (Table S1). This result represents an unprecedented level of performance, far beyond any previously reported in the literature. This becomes even clearer when considering our previous studies using both diluted¹⁷ and concentrated²⁰ ammonia feeds, where combined modelling and experimental results demonstrated that space velocities as low as 2500 $\text{NI/kg}_{\text{cat/h}}$ are required to achieve complete conversion of pure NH_3 below 500 °C in a conventional packed-bed reactor. The present modelling analysis identifies H_2 scavenging as a highly effective strategy for fully overcoming the kinetic and reactor performance limitations.

3.3 O_2 cofeeding tests as experimental verification

Given the remarkable impact and implications of the modelling results, experimental verification of the potential enhancement of the catalytic performance was pursued to validate the concept. A strategy of chemical scavenging was adopted. Oxygen (O_2) was selected as the simplest scavenger, thus the simplest diagnostic tool to obtain and reveal the effect of H_2 removal, as H_2 can react with O_2 via oxidation yielding only water as the product. Accordingly, H_2 oxidation experiments were first performed over the same 1 wt% Ru/MgAl₂O₄ catalyst. The results (Fig. 4) demonstrate that H_2 oxidation proceeds substantially faster than NH_3 decomposition, thereby confirming that, upon cofeeding O_2 with NH_3 , the H_2 generated from NH_3 decomposition can be rapidly consumed by O_2 .



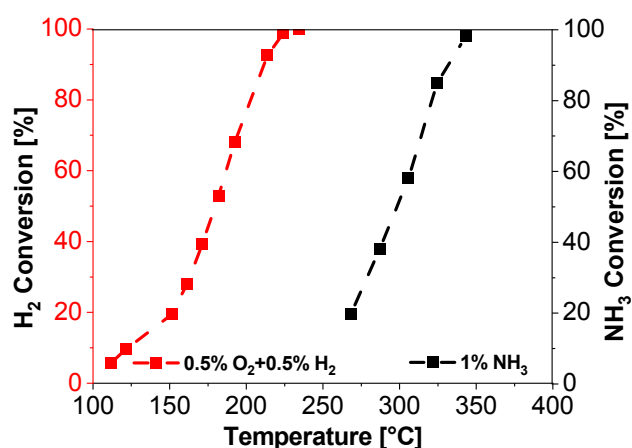
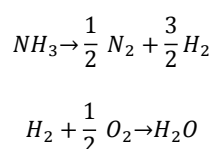


Fig. 4 H₂ oxidation (red, left y-axis) vs. NH₃ decomposition (black, right y-axis)

Subsequently, NH₃ decomposition experiments were conducted using an NH₃/He feed supplemented with 0.05–0.25% O₂, under the assumption that the introduced O₂ would efficiently remove surface H* species in accordance with the following consecutive reaction scheme:



As H₂ oxidation is an exothermic process, higher O₂ concentrations were not employed to prevent heat release from affecting the reaction temperature. The actual reactor temperatures measured by an independent thermocouple deviated by only 0.7 °C from the oven setpoints (Fig. S1), which is considered negligible.

The red squares in Fig. 3 present experimentally measured NH₃ conversions at the very temperatures where complete O₂ conversion and no H₂ production were observed. These points correspond to the exact balance between H₂ production via NH₃ decomposition and H₂ consumption through oxidation. Notably, for the 1% NH₃ + 0.05%–0.25% O₂ mixtures, the measured NH₃ conversions and temperatures closely matched the predicted ideal conversions at zero hydrogen coverage (blue line), demonstrating a pronounced rate enhancement relative to operation without O₂ cofeeding. Notably, no NO_x formation was detected under all the tested conditions.

It is also important to note that ICP–OES analysis confirmed that the Ru loading remained close to the nominal 1 wt. % value both before and after reaction, indicating negligible Ru loss during catalytic testing.

3.4 Post-reaction TPD

To further support the interpretation of the O₂ cofeeding experiments, temperature-programmed desorption under He flow was performed to identify surface species after exposure to either 1% NH₃ or 1% NH₃ + 0.25% O₂. As shown in Fig. 5, H₂ desorption was observed after the activity tests with NH₃ alone at both 250 °C and

320 °C, representative of the same temperature and of a comparable conversion level as in the O₂-cofed experiment, respectively. As reported in detail in the Supplementary, H₂ desorption was accompanied by N₂ and NH₃ signals; although a detailed analysis of the surface coverages is beyond the scope of this work, the deconvolution of signals suggests the presence of NH₃, N* and H* on the surface with H* growing with temperature, in line with the kinetic findings (Fig. S2). In contrast, after exposure to 1% NH₃ + 0.25% O₂, the H₂ signal was nearly undetectable, while traces of N₂ and NH₃ desorbed. These findings demonstrate that O₂ cofeeding effectively removes surface hydrogen species, leaving the Ru surface essentially free of adsorbed H*. The resulting surface is therefore cleaner and largely unblocked, consistently with the enhanced catalytic activity observed under O₂ cofeeding conditions.

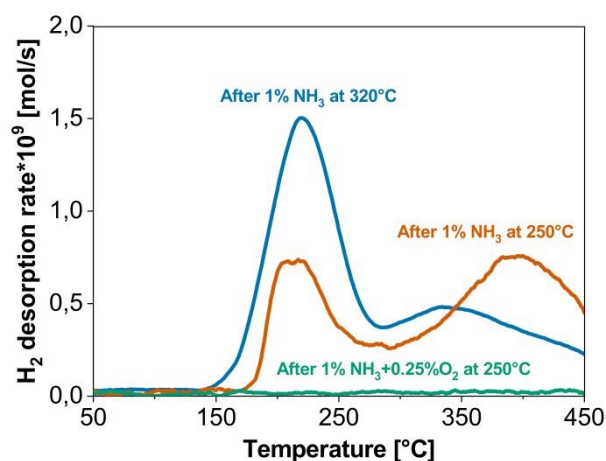


Fig. 5 Post-reaction TPD under He profiles for samples exposed to 1% NH₃ at 250 °C and 320 °C and 1% NH₃+0.25% O₂ at 250 °C.

3.5 Characterization of stability and state of the surface

The potential impact of introduced O₂ and the steam generated during O₂ cofeeding on catalyst stability has been a subject of concern. DFT-based microkinetic simulations of NH₃ decomposition over Co and Co–BaO catalysts have indicated that water impurities in NH₃ can oxidize the catalyst at low NH₃ conversion, whereas at higher conversion the produced H₂ maintains the catalyst in a reduced state.²¹ Moreover, Atsumi et al. further demonstrated experimentally that steam can deactivate Ni/Al₂O₃ catalysts for NH₃ decomposition through the formation of NiAl₂O₄.²²

The stability of the Ru/MgAl₂O₄ catalyst and the state of the surface under O₂ cofeeding conditions were thus thoroughly investigated. As shown in Fig. 6, the NH₃ conversion (1 % NH₃, 320 °C) remained essentially constant over 15 days of testing during which the catalyst was exposed to varying O₂ concentrations. These results demonstrate that, under the conditions investigated, neither the introduced O₂ nor the steam formed during O₂ cofeeding compromised catalyst stability.



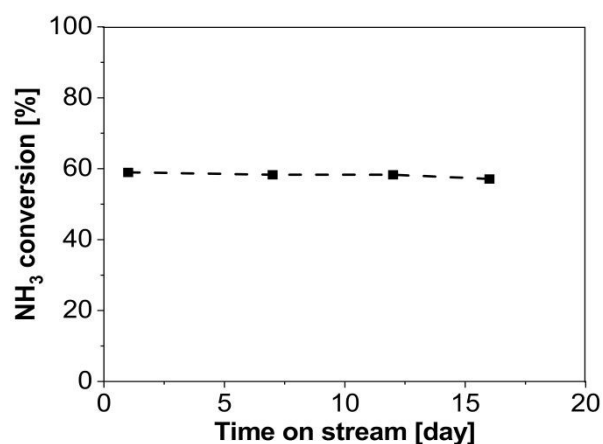


Fig. 6 Catalyst stability test under 1% NH₃ at 320°C

Several characterization techniques were employed to investigate the catalyst surface state after varying treatments.

XRD - XRD patterns were collected for the fresh catalyst as well as the catalysts after reaction under 1% NH₃ and 1% NH₃ + 0.25% O₂ atmospheres. As shown in Fig. 7, all three samples exhibited similar patterns, with diffraction peaks corresponding to metallic Ru, while no RuO₂ phase was detected. These results strongly support that the catalyst remained in the metallic state and was not oxidized after reaction under 1%NH₃ + 0.25%O₂ at 250°C. The Ru crystallite size was estimated by the Scherrer equation, yielding values of 10-11 nm both for the fresh catalyst and the spent samples.

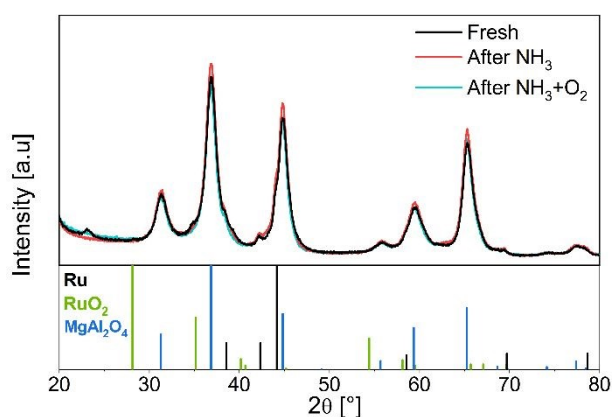


Fig. 7 XRD patterns of fresh catalyst (black), catalyst after reaction with 1% NH₃ (red) and catalyst after reaction with 1% NH₃+0.25% O₂ (light blue).

Electron microscopy – HAADF-STEM images are reported in Fig. 8 for the fresh and spent samples; they reveal that the Ru particles are partially overlapped, being embedded in the aluminates structure, and often of arbitrary shape; this makes an accurate estimation of individual particle sizes challenging. One of their dimensions appears to be in the range of 10-15 nm, with extreme values spanning from 5 to 40 nm. In line with XRD analyses, no change in Ru crystallite size was noticeable, further supporting that the reacting conditions did not produce samples restructuring.

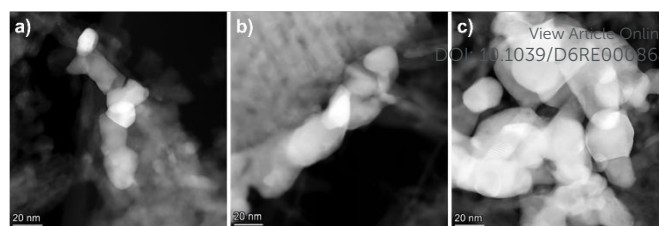


Fig. 8 HAADF-STEM images of a) fresh catalyst; b) catalyst after reaction with 1% NH₃; c) catalyst after reaction with 1% NH₃+0.25% O₂

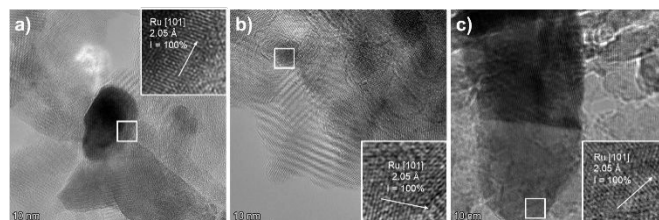


Fig. 9 HRTEM images of a) fresh catalyst; b) catalyst after reaction with 1% NH₃; c) catalyst after reaction with 1% NH₃+0.25% O₂

HRTEM images were also obtained for the above-mentioned three samples. Fig.9 clearly shows that the particles located on the MgAl₂O₄ support exhibit lattice fringes characteristic of metallic Ru, both on the bulk and on their surface. The measured interplanar spacing for the most intense reflexes of metallic Ruthenium differs significantly from those reported for Ru oxides and MgAl₂O₄, confirming the absence of surface RuO_x species.

H₂-TPR - Hydrogen temperature-programmed reduction measurements were performed to further assess the state of Ru before and after exposure to O₂. As shown in Fig. 10, the H₂ uptake following treatment of the catalyst with 1% NH₃ + 0.25% O₂ at 250 °C is slightly higher than that observed after exposure to 1% NH₃ alone under the same conditions. In contrast, the H₂ consumption after the TPO-treatment is significantly greater than in the aforementioned cases. These results indicate that substantial oxidation of the catalyst occurs during TPO, whereas no meaningful oxidation takes place under NH₃ or NH₃+O₂ treatments. The H₂ uptake observed in the latter cases is likely attributable to H₂ adsorption, given the strong affinity of Ru for hydrogen. The slightly increased H₂ uptake after exposure to 1% NH₃ + 0.25% O₂ relative to NH₃ alone may result from



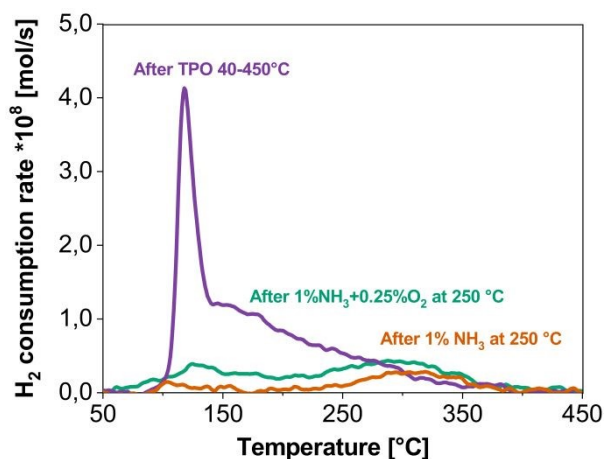


Fig. 10 H₂ TPR profiles recorder after pre-treatment under 1% NH₃, 1% NH₃+0.25% O₂, and TPO conditions.

surface cleaning by O₂, which generates a greater number of accessible sites for H₂ adsorption. This interpretation aligns with the catalytic stability results and the surface characterization, further confirms that low-level O₂ cofeeding does not induce Ru oxidation nor compromise catalyst performance.

The bulk of the data allows to conclude that the enhancement of NH₃ conversion can be unambiguously attributed to the H₂-scavenging effect induced by O₂ cofeeding.

3.6 H-scavenging: catalyst scale vs reactor scale

At the catalyst scale, formulations and preparation strategies that weaken Ru–H interactions are expected to facilitate surface H-scavenging, leading to breakthrough improvements in low-temperature activity. This approach has been pursued by Yan et al.¹⁵ through the development of Ru/CeO₂ catalysts, where the formation of oxygen vacancies enhances the mobility of surface H* species, allowing their transfer from Ru sites to the support as –OH groups.

However, if H₂ remains present in the gas phase, then despite the enhanced catalytic activity, the reactor will still be constrained by the thermodynamics of the reaction. As a result, increasing the operating pressure will limit the attainable maximum conversion, as illustrated in Fig. 11.

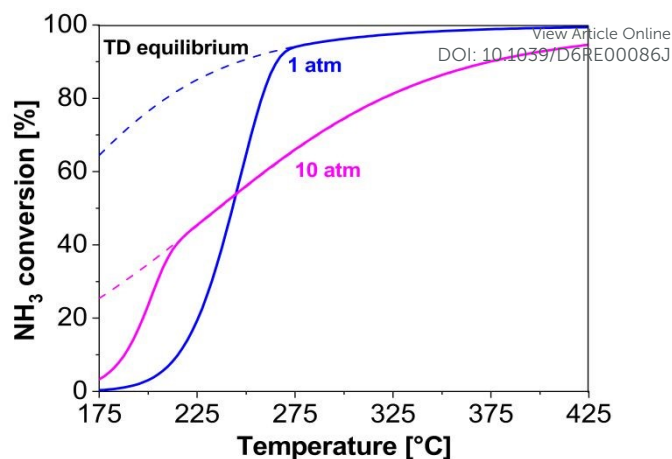


Fig. 11 Predicted performance at zero H* coverage ($K_{H_2} = 0$ in Eq. 4) but accounting for thermodynamic equilibrium ($\eta \neq 0$). Pure NH₃ feed at 1 and 10 atm (GHSV = 20,000 NI/kg_{cat}/h).

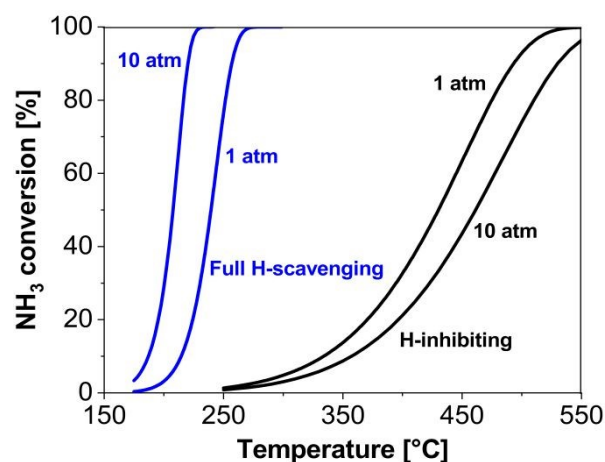


Fig. 12 Predicted effect of pressure in the ideal case of full H₂-scavenging (blue curves, $K_{H_2} = 0$ and $\eta = 0$ in Eq. 4) compared with the predicted effect of pressure in the conventional H₂-inhibited kinetic regime. Pure NH₃ feed, GHSV = 20,000 NI/kg_{cat}/h.

The analysis shows the benefits and limits that are inherently bound to a H-scavenging strategy at the catalyst scale, if gas-phase H₂ is retained in the reactor. Conversely, at the reactor scale, complete removal of H₂ from the gas phase can simultaneously unlock the full catalytic potential and eliminate thermodynamic limitations. This is clearly demonstrated in Fig. 12, which compares the performance of a conventional packed-bed reactor to that of an ideal reactor under complete H₂ removal operating with pure NH₃ at 1 and 10 atm. Although these cases represent idealized conditions, the improvement in the conversion–temperature relationship is striking. The simulations highlight the transformative potential of the H₂-scavenging strategy converting the traditionally negative pressure effect into a positive one and thus pave the way for genuine process intensification.

In principle, H₂ scavenging at the reactor scale can be achieved by integrating the catalytic bed with selective membranes that continuously remove hydrogen via permeation. Pd-based membranes represent state-of-the-art for H₂ purification and have



been extensively investigated in combination with catalytic H₂ production processes.²³ In line with this approach, several studies have explored the use of membrane reactors for NH₃ decomposition, primarily focusing on (i) the purity of the permeated H₂ and (ii) the expected thermodynamic advantage derived from Le Chatelier's principle.^{24, 25} However, existing studies on membrane-assisted NH₃ decomposition have largely overlooked the intrinsic kinetic limitations of the reaction, thereby missing the proper formulation of the problem. To the best of our knowledge, no prior work has addressed membrane reactor design from a kinetic perspective, nor has it been guided by the principle presented here. This principle clearly points toward maximizing the local H₂-removal rate, rather than optimizing for overall H₂ purity. The scavenging efficiency is thus governed by kinetic parameters, not by H₂/N₂ selectivity or thermodynamic equilibria, since the reaction is kinetically controlled.

While current membrane research continues to focus on achieving high performance and, critically, long-term stability, the present study suggests that the development and operation of an effective H₂-scavenging system could enable membrane reactors to function at dramatically lower temperatures (< 300 °C) than those typically reported. This represents a major paradigm shift, as integrating membranes with high-temperature catalytic systems has long been recognized as a significant technological challenge.

4. Conclusions

In summary, this study demonstrates that a vast potential for improving NH₃-decomposition kinetics lies in the effective removal of both surface-bound and gas-phase hydrogen species. The concept of H₂ scavenging was experimentally validated through simple yet conclusive diagnostic O₂ cofeeding tests.

The experimental findings showed the remarkable promotion of ammonia decomposition rate produced by H₂ removal from the Ru sites. Notably, even greater activity enhancements can be foreseen at high pressures, since the H₂-inhibited kinetics of Ru exhibit negative global order, whereas the kinetics of H₂-clean surfaces have positive order and positive pressure dependence, which opens to process intensification. For practical applications of the principle, however, solutions other than O₂ cofeeding are needed to preserve H₂ productivity.

Indeed, the modelling and experimental results open the path toward the design of new catalyst formulations that mitigate H*-poisoning by weakening Ru-H interactions and enhancing H* mobility. It also opens to the development of multifunctional reactors in which H₂ is continuously withdrawn from the gas phase at a rate precisely balanced with its generation. Recent advances in Ru/CeO₂ catalysts and membrane reactor technologies align with this approach and highlight ongoing progress. However, the present study provides the critical framework for predicting the maximum achievable performance, offering essential insights for engineering design and optimization. Most importantly, the H₂-scavenging principle paves the way for a variety of alternative reactors and process concepts that employ different driving forces for hydrogen removal, leveraging NH₃ as a hydrogen carrier for both energy and chemical applications. These include hydrogen uptake into metal

hydrides, chemical consumption via hydrogenation reactions, and proton removal in electrochemical cells, defining a vast and promising landscape for future innovation in chemical reaction engineering.

Author contributions

Yi Qiu: conduction experiments, data curation, writing the original draft. Ivan Conti: conduction experiments, data curation, modelling, reviewing and revising the manuscript. Enrico Berretti: conduction experiments, data curation, reviewing and revising the manuscript. Alessandra Beretta: supervision, reviewing and revising the manuscript.

Conflicts of interest

There are no conflicts to declare.

Data availability

The data supporting this article have been included as part of the Supplementary Information.

Acknowledgements

The authors gratefully acknowledge the support of a PhD fellowship for Yi Qiu from the China Scholarship Council (CSC).

References

- M. D. Allendorf, V. Stavila, J. L. Snider, M. Witman, M. E. Bowden, K. Brooks, B. L. Tran, T. Autrey, *Nat. Chem.* 2022, **14**, 1214.
- T. He, P. Pachfule, H. Wu, Q. Xu, P. Chen, *Nat. Rev. Mater.* 2016, **1**, 16059.
- M. Asif, S. S. Bibi, S. Ahmed, M. Irshad, M. S. Hussain, H. Zeb, M. K. Khan, J. Kim, *Chem. Eng. J.* 2023, **473**, 145381.
- D. R. MacFarlane, P. V. Cherepanov, J. Choi, B. H. Suryanto, R. Y. Hodgetts, J. M. Bakker, F. M. F. Vallana, A. N. Simonov, *Joule*, 2020, **4** (6), 1186.
- N. Morlanés, S. P. Katikaneni, S. N. Paglieri, A. Harale, B. Solami, S.M. Sarathy, J. Gascon, *Chem. Eng. J.* 2021, **408**, 127310.
- <https://www.topsoe.com/ammonia-cracking>
- <https://ammoniaenergy.org/articles/kier-unveils-improved-ammoniocracking-system/>
- J.C. Ganley, F.S. Thomas, E.G. Seebauer, R.I. Masel, *Catal. Lett.* 2004, **96**, 117.
- S.F. Yin, B.Q. Xu, X.P. Zhou, C.T. Au, *Appl. Catal. A: Gen.* 2004, **277**, 1.
- I. Lucentini, X. Garcia, X. Vendrell, J. Llorca, *Ind. Eng. Chem. Res.* 2021, **60**, 18560.
- T. Su, B. Guan, J. Zhou, C. Zheng, J. Guo, J. Chen, Y. Zhang, Y. Yuan, W. Xie, N. Zhou, H. Dang, B. Xu, Z., *Energy Fuels* 2023, **37**, 8099.



- 12 A.M. Karim, V. Prasad, G. Mpourmpakis, W.W. Lonergan, A.I. Frenkel, J.G. Chen, D.G. Vlachos, *J. Am. Chem. Soc.* 2009, **131**, 12230.
- 13 V. Prasad, A.M. Karim, A. Arya, D.G. Vlachos, *Ind. Eng. Chem. Res.* 2009, **48**, 5255.
- 14 M. C.J. Bradford, P. E. Fanning, M.A. Vannice, *J. Catal.* 1997, **172**(2), 479.
- 15 L. Yan, X. Fu, W. Wang, C. Jia, *Appl Catal. B: Environ. En.* 2025, **378**, 125538.
- 16 W. J. Movick, F. Kishimoto, K. Takanabe, *Chem. Eng. J.* 2023, **452**, 139525.
- 17 Y. Qiu, F. S. Franchi, N. Usberti, A. Beretta, *Fuel Proc. Technol.* 2025, **276**, 108270.
- 18 S. Sayas, N. Morlanés, S.P. Katikaneni, A. Harale, B. Solami, J. Gascon, *Catal. Sci. Technol.* 2020, **10**, 5027.
- 19 L. J. Gillespie and J. A. Beattie, *Phys. Rev.* 1930, **36**, 743–753
- 20 F. S. Franchi, M. Ambrosetti, N. Usberti, A. Beretta, G. Groppi, E. Tronconi, *Appl. Catal., A* 2026, **709**, 120664.
- 21 Z. Almisbaa, P. Sautet, *J. Catal.* 2025, 446, 116054.
- 22 R. Atsumi, R. Noda, H. Takagi, L. Vecchione, A. D Carlo, Z. D. Prete, and K. Kuramoto, *Ind. Eng. Chem. Res.* 2014, **53**, 17849–17853.
- 23 V. Piemonte, L. Di Paola, M. De Falco, A. Iulianelli, A. Basile, In *Advances in Hydrogen Production, Storage and Distribution* (Eds.: A. Basile, A. Iulianelli) Elsevier Science: Amsterdam, The Netherlands, 2014, 283–316
- 24 V. Cecchetto, L. di Felice, F. Gallucci, *Energy Fuels* 2023, **37**, 10775.
- 25 E. S. Napolitano, C. Italiano, A. Brunetti, M. Thomas, A. Vita, G. Barbieri *Fuel. Proc. Technol.* 2025, **272**, 108203.

View Article Online
DOI: 10.1039/D6RE00086J

Open Access Article. Published on 11 June 2026. Downloaded on 6/11/2026 11:34:55 PM.
This article is licensed under a Creative Commons Attribution 3.0 Unported Licence.



The supporting data has been provided as part of the Supplementary information. [View Article Online](#)
DOI: 10.1039/D6RE00086J

Supplementary information:

- Tables S1 reports the Quantitative comparison between the cases of H₂-inhibited and H₂-scavenged kinetics,
- Fig. S1 demonstrates the negligible impact of O₂-cofeed on the catalyst best temperature.
- Fig. S2a presents the species observed during He-TPD over the catalyst pretreated with 1% NH₃ at 250 °C (corresponding to ~10% NH₃ conversion) with detailed description of the deconvoluted signals.

